Solid-state NMR and EPR Spectroscopy of Mn2+-Substituted ATP-Fueled Protein Engines

Author(s):
Wiegand, Thomas; Lacabanne, Denis; Keller, Katharina; Cadalbert, Riccardo; Lecoq, Lauriane; Yulikov, Maxim; Terradot, Laurent; Jeschke, Gunnar; Meier, Beat H.; Böckmann, Anja

Publication date:
2017-03-13

Permanent link:
https://doi.org/10.3929/ethz-b-000128825

Originally published in:
Angewandte Chemie. International Edition 56(12), https://doi.org/10.1002/anie.201610551

Funding acknowledgement:
159707 - NMR studies in the Solid State (SNF)
146757 - NMR studies in the Solid State (SNF)
169057 - Generation of spin-label based restraints on biomolecular structure and their use in hybrid structure modelling (SNF)

Table of Contents

Materials and Methods

HpDnaB samples for solid-state NMR

^{13}C-^{15}N labelled *Hp*DnaB was prepared in buffer A (2.5 mM sodium phosphate, pH 7.5, 130 mM NaCl) as described in reference.[1] Deuterated DnaB was prepared using the same protocol, but the protein was expressed in deuterated media. The buffer was exchanged by the corresponding D_2O buffer before nucleotide addition.

HpDnaB:AMP-PNP:Mg^{2+} complex

0.3 mM *Hp*DnaB (all concentration are given with respect to an *Hp*DnaB monomer) in buffer A was mixed with 5 mM $MgCl_2 \cdot 6H_2O$ and, consecutively, with 5 mM AMP-PNP (18-fold molar excess of AMP-PNP compared to an *Hp*DnaB monomer) and incubated for 2 h at 4°C. The protein solution was sedimented[1-4] in the MAS-NMR rotor (16 h at 4°C with 210000 g acceleration) using home-build tools.[5] Amino-acids, Na_3VO_4, AMP-PNP and ATP were purchased from Sigma-Aldrich for all preparations.

HpDnaB:AMP-PNP:Mn^{2+} complex

0.3 mM *Hp*DnaB in buffer A was mixed with 1.4 mM $MnCl_2 \cdot 6H_2O$ (5-fold molar excess compared to an *Hp*DnaB monomer) and, consecutively, with 5 mM AMP-PNP (18-fold molar excess of AMP-PNP compared to an *Hp*DnaB monomer) and incubated for 2 h at 4°C. The protein solution was sedimented[1-4] in the MAS-NMR rotor (16 h at 4°C with 210000 g acceleration) using home-build tools.[5] Lower ratios of Mn^{2+}:*Hp*DnaB monomer were explored additionally, but only a partial occupation of AMP-PNP binding sites was observed under these conditions.

BmrA samples for solid-state NMR

Production, purification and reconstitution in homemade lipids of the membrane protein ^{12}C-^{14}N-[LVIKHP]-^{13}C-^{15}N-BmrA was achieved as described by Kunert *et al.*[6] In order to perform the reverse unlabelling, natural abundance Leu (0.23g/L), Val (0.23g/L), Ile (0.23g/L), Lys (0.40g/L), His (0.40g/L), Pro (0.10 g/L) were added in the culture medium one hour before the induction. For the purification, the concentration of the protein did never exceed 1mg.mL^{-1} (17µM) to avoid aggregates. The protein was diluted for the membrane reconstitution to 0.25 mg.mL^{-1} (4.25 µM).

Drug transport activity of BmrA in presence of Mn^{2+} or Mg^{2+}

The experimental procedures are described in Steinfels *et al*.[7] Briefly, in a 1 mL cuvette, 100 µg of inverted membrane vesicles from *E. coli* C41(DE3) overexpressing BmrA were incubated

in presence of 2 mM ATP and ATP regeneration buffer (4mM phosphoenolpyruvate, 60µg.mL^{-1} pyruvate kinase). After 1 minute at 25 °C incubation, 10 µM doxorubicin were added and the transport-reaction was started by the addition of 2mM of Mg^{2+} or Mn^{2+}. The excitation and emission wavelengths were, respectively, 480 and 590 nm.

BmrA:ADP:Mg^{2+}:VO_4^{3-} complex

The lipid-reconstituted protein was mixed with 1 mM Na_3VO_4 and with 5 mM ATP-Mg corresponding to a 1500-fold molar excess of ATP-cation compared to a BmrA monomer. All compounds were prepared in 50 mM Tris-HCl pH 8.0, 200 mM NaCl and 5% glycerol, and the preparations were incubated for 2 h at room temperature. The protein in lipids was sedimented in the MAS-NMR rotor (1 h at 4°C with 120000 g acceleration) using home-build tools.[5]

BmrA:ADP:Mn^{2+}:VO_4^{3-} complex

The lipid-reconstituted protein was mixed with 1 mM Na_3VO_4 and with 1 mM ATP-Mn corresponding to a 300-fold molar excess of ATP-cation compared to a BmrA monomer. Lower and higher ratios of Mn^{2+}:BmrA monomer were explored additionally, but a partial occupation of ATP:Mn^{2+} binding sites or global signal loss, respectively, was observed under these conditions. All compounds were prepared in 50 mM Tris-HCl pH 8.0, 200 mM NaCl and 5% glycerol, and the preparations were incubated for 2 h at room temperature. The protein in lipids was sedimented in the MAS-NMR rotor (1 h at 4°C with 120000 g acceleration) using home-build tools.[5]

Experimental details of solid-state NMR experiments

Solid-state NMR spectra were acquired at 18.8 T and 20.0 T static magnetic field strength using 3.2 mm Bruker Biospin "E-free" probes. The MAS frequency was set to 17.5 and 17.0 kHz, respectively. The sample temperature was set to 278 K.[5] The spectra were processed with the software TOPSPIN (version 3.2, Bruker Biospin) with a shifted (2.5 to 3.0) squared cosine apodization function and automated baseline correction in the direct dimension. All spectra were analyzed with the software CcpNmr[8] and referenced to 4,4-dimethyl-4-silapentane-1-sulfonic acid (DSS). The assignments of *Hp*DnaB and *Hp*DnaB:AMP-PNP:Mg^{2+} are according to references.[9,10] PRE effects were extracted from 2D and 3D spectra and the ratios I_{para}/I_{dia} were scaled such that the average I_{para}/I_{dia} value for resonances of the NTD is one (the NTD is not participating in nucleotide binding). This allows for a compensation of experimental errors resulting from different experimental conditions in different measurement time periods. The error bars shown in Figure 2b are based on Gaussian error propagation and estimated from the noise levels in the corresponding spectra.

_Hp_DnaB samples for CW-EPR

HpDnaB:AMP-PNP:Mn^{2+} complex

3.6 mM *Hp*DnaB in buffer A was mixed with 0.3 mM $MnCl_2 \cdot 4H_2O$ and consecutively 5 mM AMP-PNP (18-fold molar excess of AMP-PNP compared to an *Hp*DnaB monomer) and incubated for 2 h at 4°C.

$MnCl_2$:AMP-PNP reference solution

A 0.3 mM $MnCl_2 \cdot 4H_2O$ and 5mM AMP-PNP solution in buffer A was prepared.

CW EPR spectra were measured for a sample with 12-fold excess of the *Hp*DnaB monomers with respect to the Mn^{2+} ions, in order to ensure predominant presence of the metal ions in the form of *Hp*DnaB:AMP-PNP:Mn^{2+} complexes. In this case, most of protein oligomers should have only one Mn^{2+} ion bound. Note that the CW EPR spectrum of Mn^{2+} ions is dominated by the metal ion ligands and magnetic nuclei in the close vicinity. Unless the distances to the next neighbor Mn^{2+} species are below 2 nm, the interaction with other metal centers can be neglected. As the Mn^{2+} EPR spectrum is not dominated by the paramagnetic metal ions in close vicinity, it should not differ between this sample and the sample with all NBDs loaded with Mn^{2+}. Additional CW experiments were performed on a sample with an *Hp*DnaB:Mn^{2+} ratio of 1:1. and are shown in Figure S2a.

BmrA samples for CW-EPR

BmrA:ATP:Mn^{2+}:VO_4^{3-} complex

2 mL of BmrA 0.25 mg/mL (3.8 μM) in buffer solution (50 mM Tris, 100 mM NaCl, 5% glycerol) was incubated with ATP:Mn^{2+} ratio 300:1 (1.140 mM ATP:Mn^{2+}) and 5 mM Vanadate solution. The sample was sedimented and washed three times with the buffer solution. The final protein concentration was ~200 μM.

ATP:Mn^{2+}:VO_4^{3-} reference solution

A 1 mM ATP, 1 mM MnCl2·4H2O and 5mM Na3VO4 solution in 50 mM Tris, 100 mM NaCl, 5% Glycerol buffer was prepared.

For BmrA CW EPR measurements, the sample preparation was based on the slow kinetics of the Mn^{2+} dissociation from the binding sites in the NBDs. A 300-fold excess of Mn^{2+} was used to load Mn^{2+} ions into the binding site of BrmA. Then, the protein was sedimented and washed three times with the buffer solution without Mn^{2+} ions to remove unbound excess of Mn^{2+} ions as much as possible. The washing procedure took about three times five min. The spectrum is shown in Figure S16a in comparison to a reference solution of Mn^{2+} ions in the buffer at room temperature.

HpDnaB samples for pulsed EPR experiments

HpDnaB:AMP-PNP:Mn^{2+} complex

Buffer A was exchanged with the corresponding D_2O buffer (buffer B). For relaxation measurements, 0.6 mM *Hp*DnaB in buffer B was mixed with 0.6 mM $MnCl_2 \cdot 6H_2O$ and consecutively 10 mM AMP-PNP (18-fold molar excess of AMP-PNP compared to an *Hp*DnaB monomer) and incubated for 2 h at 4°C. The solution was mixed with glycerol-d_8 leading to a final protein concentration of 0.3 mM. For the DEER experiments, a deuterated sample of *Hp*DnaB was used with a 1.5-fold excess of Mn^{2+} compared to an *Hp*DnaB monomer. The samples were filled into 3 mm outer diameter quartz sample tubes and subsequently shock-frozen by immersion into liquid nitrogen.

$MnCl_2$:AMP-PNP reference solution

A 0.6 mM $MnCl_2 \cdot 4H_2O$ and 10 mM AMP-PNP solution in buffer B was prepared. The solution was diluted with glycerol-d_8 until concentrations of 0.3 mM $MnCl_2 \cdot 4H_2O$ and 5 mM AMP-PNP were reached.

$MnCl_2$ reference solution

A 0.6 mM $MnCl_2 \cdot 4H_2O$ solution in buffer B was prepared. The solution was diluted with glycerol-d_8 (final $MnCl_2 \cdot 4H_2O$ concentration of 0.3 mM).

The protein-containing and reference samples were dissolved in buffer B:glycerol-d_8 (1:1 v:v). Samples are filled into 3 mm outer diameter quartz sample tubes and subsequently shock-frozen by immersion into liquid nitrogen. Pulsed EPR measurements were done on a sample with 1:1 ratio between Mn^{2+} ions and *Hp*DnaB monomers for echo-detected (ED) field-swept and relaxation measurements, and with 1.5:1 ratio between Mn^{2+} ions and *Hp*DnaB monomers for distance measurements in order to obtain a sufficiently large fraction of multiply metal-loaded *Hp*DnaB oligomers. For significantly lower relative amounts of *Hp*DnaB, the fraction of Mn^{2+} ions not bound to the NBDs would be too high, resulting in a too low dipolar modulation depth in the DEER measurements. For significantly higher *Hp*DnaB amounts the fraction of protein oligomers with only one Mn^{2+} ion bound would increase, again reducing the dipolar modulation depth in the DEER experiment. Despite the presence of, on average, six Mn^{2+} ions per protein complex, multi-spin effects are negligible due to the modulation depth of only about 1% even when using ultra-wideband pump pulses.

BmrA samples for pulsed EPR experiments

BmrA:ATP:Mn^{2+}:VO_4^{3-} complex

1 mL of BmrA 0.25 mg/mL (3.8 µM) in 50 mM Tris, 100 mM NaCl, 5% Glycerol was incubated with ATP-Mn^{2+} ratio 300:1 (1.140 mM ATP-Mn^{2+}) and 5 mM Vanadate solution. The sample was sedimented and resuspended with 40 µL of buffer containing 50% glycerol (50 mM Tris, 100 mM NaCl, 50% Glycerol incubated).

$MnCl_2$:ATP reference solution

A 100 µM ATP and 100 µM $MnCl_2 \cdot 4H_2O$ solution in 50 mM Tris, 100 mM NaCl, 50% Glycerol buffer was prepared.

For BmrA, the sample preparation was based on the slow kinetics of the Mn^{2+} dissociation from the binding sites in the NBDs (vide supra). Compared to the CW samples, the protein was centrifuged and the buffer was exchanged by the pure buffer/glycerol mixture without Mn^{2+} ions, without washing. Samples were then transferred to 3 mm outer diameter quartz tubes and immediately frozen by immersion into liquid nitrogen, and were kept frozen during handling and DEER measurements to avoid any kinetic effects occurring during sample preparation and measurement.

Experimental details of CW-EPR experiments

CW X-band EPR spectra were detected using a Bruker EMX spectrometer equipped with a Bruker Elexsys Super High Sensitive probehead. Measurements were performed at room temperature, 100 kHz field modulation, 250 to 450 mT field sweep, 4 G modulation amplitude, and 1 mW microwave power (10 dB attenuation). The time constant was 10.24 ms and the conversion time 40.96 ms. The samples were filled into 0.9 mm inner diameter glass capillaries (10-20 µl sample volume).

Experimental details of pulsed EPR experiments

Pulsed experiments were performed on a customized Bruker Elexsys E580 Q-band spectrometer,[11] which is extended with an incoherent ultra-wide band (UWB) pulse channel based on a 12 GS/s arbitrary waveform generator (AWG, Agilent M8190A).[12] The temperature was adjusted, using a helium flow cryostat, to 10 K for distance measurements and to 20 K for ED field-swept and relaxation measurements. ED field-swept and relaxation measurements were performed at 20 K for samples related to *Hp*DnaB and 10 K for BmrA.

ED field-swept spectra were acquired with a Hahn-echo pulse sequence t_p–τ–2t_p–τ–echo using a pulse length t_p = 12 ns and τ = 400 ns. The same sequence was used to record the phase

memory decay by incrementing the initial interpulse delay τ in steps of 240 ns and 40 ns for samples related to DnaB and BmrA, respectively.

Relaxation traces were detected in the valley between the 2nd and 3rd hyperfine line of the Mn^{2+} EDEPR spectra marked by an arrow in Figure S2b for *Hp*DnaB and Figure S16b for BmrA. The reason for this choice is the larger difference in linewidths for the central $|+1/2\rangle\leftrightarrow|-1/2\rangle$ transitions of different species as compared to the difference in widths for any other transition of the high-spin Mn^{2+} ions. The six sharp lines of the Mn^{2+} EPR spectrum correspond to the central $|+1/2,M_I\rangle\leftrightarrow|-1/2,M_I\rangle$ transition and are split by the ^{55}Mn hyperfine coupling (natural abundance 100%, nuclear spin I=5/2). Considering the zero-field splitting (ZFS) term in the spin Hamiltonian as a small perturbation to the electron Zeeman interaction, in first (linear) order of a perturbation series this transition is not affected by the ZFS term, while all other transitions of Mn^{2+} are broadened by the orientation dependent ZFS interaction. In second order of the perturbation series the central transition of Mn^{2+} gets moderately broadened by the ZFS term. Thus, the dependence of the width of this transition on ZFS is steeper than for all other transitions. As a result, the intensity of the spin echo signal per fixed amount of molecules, measured at this transition, would differ to the largest extent for different Mn^{2+} species detected in our experiments. In the valley between any two hyperfine components of the central transition, the relative contributions of different species to the spin echo signal correspond more closely to their concentrations in the sample. Among all possible positions, the selected one corresponded to the maximum spin-echo intensity.

Determination of the fraction of bound Mn^{2+} by EPR relaxation measurements

Transverse relaxation of Mn^{2+} ions is strongly affected by the interaction with other paramagnetic centers, as well as with surrounding nuclear spins, via the spin diffusion mechanism. Among all nuclear spins, matrix protons contribute by far most strongly, if they are present. For the *Hp*DnaB system this allows for a relaxation-based separation of the Mn^{2+} centers in the form of AMP-PNP:Mn^{2+} from the ones bound to the protein. By measuring the *Hp*DnaB:AMP-PNP:Mn^{2+} sample in deuterated buffer/deuterated glycerol mixture a very low number of solvent protons in the vicinity of free AMP-PNP:Mn^{2+} species was ensured. For these species the protons in the vicinity of Mn^{2+} originated only from the very limited number of the AMP-PNP protons, whereas other nearby magnetic nuclei had much smaller gyromagnetic ratios and, accordingly, their flips contributed much less to the electron spin transverse relaxation. Binding of the AMP-PNP:Mn^{2+} complex to the protein brings the Mn^{2+} ions in close vicinity of a large pool of protons. This and the presence of several Mn^{2+} ions

close to each other in the *Hp*DnaB:AMP-PNP:Mn^{2+} species leads to a faster relaxation of the bound species as compared to unbound AMP-PNP:Mn^{2+} species. Since in the protein-containing sample both types of species were present, the actual transverse relaxation decay trace shows a complex behavior with quick initial decay, due to the bound species, and a significantly slower decaying tail due to the unbound species.

This phenomenon allows, in the case of *Hp*DnaB, to rather accurately estimate the fraction of Mn^{2+} ions attached to the protein NBDs. We can assume, in the same way as in an analogous longitudinal relaxation data analysis for lanthanide-radical pairs, that the additional relaxation channel for the protein-bound species is independent from all other channels, and the total relaxation rate is a sum of the rates for all relevant relaxation channels.[13,14] Under this assumption, division of the transverse relaxation time trace of the protein-containing sample by the corresponding trace for the sample with only AMP-PNP:Mn^{2+} species present, results in a ratio trace that contains a contribution from *Hp*DnaB:AMP-PNP:Mn^{2+}, which decays with the rate corresponding only to the additional relaxation channel, while the unbound AMP-PNP:Mn^{2+} species contributes constant intensity. In reality, due to intermolecular interactions, and, perhaps, due to imperfect additivity of different relaxation rates, this latter signal is not constant, but rather decays very slowly, as it is seen in the Figure 1b of the main text. Still, we can rather accurately estimate the fraction of *Hp*DnaB:AMP-PNP:Mn^{2+} species to be between the vertical coordinate of the kink of the division trace and the point where the prolongation of the slowly relaxing part of the division trace crosses the y-axis. One can see from Figure 1b that the relative intensity of the AMP-PNP:Mn^{2+} species is thus about 0.4, which corresponds to about 60 % of the *Hp*DnaB:AMP-PNP:Mn^{2+} species in the stoichiometric mixture.

For BmrA, a detailed analysis is hampered by the unknown Mn^{2+} excess resulting from sedimentation and buffer replacement. Still, on can estimate the fraction of Mn^{2+} bound to the protein in the sample to 8% of the Mn^{2+} ions within the sample (see Figure S16c).

Experimental details of DEER experiments and additional discussion of the results

The four-pulse DEER data were obtained using the sequence $\pm(\pi/2)_{obs} - \tau_1 - (\pi)_{obs} - (\tau_1 + t) - (\pi)_{chirp} - (\tau_2 - t) - (\pi)_{obs} - \tau_2 -$ echo. For DnaB, a τ_1 = 400 ns and τ_2 = 5000 ns was used. For BmrA τ_1 was set to 600 ns and τ_2 to 1400 ns. The time *t* was incremented in steps of 8 ns. The $(\pi)_{chirp}$ chirp pulse settings were analogous to the previously reported Gd^{3+}-Gd^{3+} DEER measurements.[15] The observation pulses had a length of 12 ns and the observation frequency was placed in the valley between the 2nd and 3rd hyperfine line of the Mn^{2+} at about 34.5 GHz. The linearly frequency swept (chirp) pump pulses originated from the AWG. To describe the

chirp pulses used in this work, we refer to the start and end frequencies of the frequency sweep as f_1 and f_2, respectively. Thus the sweep width Δf is the absolute difference between f_1 and f_2. Two chirp pump pulses were applied with lengths of 50 ns on both sides of the observer frequency and the pulse edges were smoothened with a quarter sine wave during 10 ns.

For *Hp*DnaB, two different sweep ranges were tested. First a sweep range from $f_1 = -0.6$ GHz to $f_2 = -0.2$ GHz and $f_1 = 0.6$ GHz to $f_2 = 0.2$ GHz with respect to the observer frequency, corresponding to a total pump bandwidth of 0.8 GHz (data shown in the top three subplots of Figure S4) and a second sweep range from $f_1 = -0.8$ GHz to $f_2 = -0.2$ GHz and $f_1 = 0.8$ GHz to $f_2 = 0.2$ GHz with respect to the observer frequency, corresponding to a total pump bandwidth of 1.2 GHz (data shown in the middle three subplots of the Figure S4). The pump pulses with a total bandwidth of 0.8 GHz resulted in a modulation depth of about 1%, while with the latter pulse settings a modulation depth of approximately 1.5% could be achieved (see Figure S4). The data in the main text (Figure 1c and d) and in the bottom three subplots in the Figure S4 show the average of both data sets.

Experiments were performed on the deuterated *Hp*DnaB sample to prolong the accessible distance range. A comparison of phase memory times of deuterated and protonated *Hp*DnaB samples is shown in Figure S3. Due to the difference in the phase memory time between NBD-bound and free Mn^{2+} species, the dipolar modulation depth was decreasing with the increase of the transverse evolution time in the DEER experiment. Furthermore, it is possible that, due to the faster transverse relaxation times of the oligomers with higher number of bound Mn^{2+} ions, the longer distance peaks are also partially reduced in intensity, similar to the earlier results of Schiemann and coauthors.[16,17]

Despite the use of broad-band pump pulses and the presence of multiple Mn^{2+} ions in each protein oligomer, the detected depth of dipolar modulation of only approximately 1% (Figure 1d) is comparable to the earlier reports on doubly Mn^{2+} labeled molecules, where modulation depths of 0.4% and 1-2% were detected for the DEER setups with narrower-band rectangular pump pulse.[18,19] Here, apparently, the factors that increase the dipolar modulation depth are compensated by the rather large ZFS of the *Hp*DnaB:AMP-PNP:Mn^{2+} complex, and the incomplete binding of the AMP-PNP:Mn^{2+} species to the NBDs. The paramagnetic Mn^{2+} ions in the buffer solution are on average quite remote from each other at the studied ion concentrations. Thus, the DEER signal from these Mn^{2+} ions would only contribute to the slowly changing intermolecular background decay and will not add to the dipolar modulation depth. Mn^{2+}-Mn^{2+} distances within the DEER distance range stem mainly from Mn^{2+} ions loaded into NBDs. Thus, the dipolar modulation depth is limited to the fraction of the spin-echo

signal originating from only the NBD-bound Mn^{2+} ions. If these ions have faster transverse relaxation than the Mn^{2+} ions in the buffer, they contribute the less to the DEER time trace the longer this trace is. The dipolar modulation depth, which stems from these NBD-bound ions, scales according to their relative contribution to the signal, and is thus expected to decrease with increasing trace length. A longer transverse relaxation time of the AMP-PNP:Mn^{2+} species would thus further reduce the DEER modulation depth, especially for experiments with long dipolar evolution times. While a low dipolar modulation depth is more difficult to detect, it assured that in every oligomer no more than two Mn^{2+} spins were excited by the DEER pulse sequence. We can thus argue that no multi-spin effects, which would be potentially possible in such oligomer systems,[20] should be present in the reported DEER data.

Experimental data were processed using the DeerAnalysis software.[21] Distance distributions were obtained by Tikhonov-regularization using a regularization parameter of 1. In the distance distribution shown in the Figure S4 (*Hp*DnaB sample), the peak at about 3 nm (right panel) is responsible for the clearly visible fast oscillations of the DEER form factor signal (central panel). Multiple full oscillations were detected for this peak and, thus, its shape is determined with good accuracy. The other peak at the distance range 5-6.5 nm corresponds to the shallow oscillation with the minimum at about 2 μs (central panel). Only about one full period of oscillation could be detected for this peak, even with use of deuterated *Hp*DnaB. Furthermore, part of this oscillation could be incorporated into the background model, and variation of this model with the validation tool in DeerAnalysis resulted in changes of the amplitude and mean distance of this peak indicated by the grey error band in Figure 1d. More precisely, in the validation procedure the beginning of the background correction range was varied between 1000 and 2500 ns in 11 steps. Furthermore, 11 different artificial noise traces of the same average magnitude as the intrinsic noise in the DEER trace were added to this trace to verify the stability of the distance distribution to the level and realization of noise. Grey colored bands in the Figures 1d and S4 (right three panels) indicate the variation of the Mn^{2+}-Mn^{2+} distance distribution in the described validation procedure. These variations affected the peak at 3 nm much less than the peak at 5-6.5 nm. Still, for any background model tested, a peak in the range 5-6.5 nm was present although it varied in width, amplitude, and mean distance. The distance range between 5 and 6.5 nm is consistent with the homology model based Mn^{2+}-Mn^{2+} distances for the non-nearest neighbors as shown in the main text Figure 1c. Thus, only the peaks at 3 and 5-6 nm are highly significant after validation and the remaining peaks could stem from the uncertainty of background validation due to short trace length and possibly from unspecifically bound Mn^{2+} and/or some flexibility of the structure.

For BmrA, three different pulse settings were tested (see Figure S17). First a sweep range from $f_1 = -0.8$ GHz to $f_2 = -0.2$ GHz and $f_1 = 0.8$ GHz to $f_2 = 0.2$ GHz with respect to the observer frequency, corresponding to a total pump bandwidth of 1.2 GHz (data shown in the top three subplots of Figure S17), a second sweep range from $f_1 = -0.9$ GHz to $f_2 = -0.3$ GHz and $f_1 = 0.9$ GHz to $f_2 = 0.3$ GHz with respect to the observer frequency, corresponding to a total pump bandwidth of 1.2 GHz (data shown in the middle three subplots of the Figure S17) and a third sweep range from $f_1 = -0.7$ GHz to $f_2 = -0.3$ GHz and $f_1 = 0.7$ GHz to $f_2 = 0.3$ GHz with respect to the observer frequency, corresponding to a total pump bandwidth of 0.8 GHz (data shown in the bottom three subplots of the Figure S17). The pump pulse with a total bandwidth of 0.8 GHz resulted in a modulation depth of about 0.16 %, while with the pulse settings with 1.2 GHz total bandwidth resulted in a modulation depth of approximately 0.14% for a 200 MHz offset and 0.12% for 300 MHz offset between pump and observed frequency. It is important to note that the distance distribution is not altered by the pump pulse settings. The data in the main text (Figure 1e, f) show the average of both 1.2 GHz total bandwidth measurements. Primary data for this averaged data set are show in Figure S18. In this case, the low dipolar modulation depth most likely results from the large fraction of unbound Mn^{2+} ions within the sample. This modulation depth still suffices to confirm the presence of the expected Mn^{2+}-Mn^{2+} distances in the sample. For the BmrA sample, the same analysis procedure as for the DnaB measurements was performed. For the validation procedure the background range was adjusted to 200 to 350 ns in 11 steps. It confirms a mean distance of about 1.9 nm in all cases. Note that these DEER data are obtained at the limit of sensitivity and stability of the EPR spectrometer. While the additional smaller peaks in the distance distribution might indicate some non-specific binding of the Mn^{2+} ions to the protein or lipid bilayers, they might as well originate from low-frequency noise or electronic instabilities of the spectrometer. An additional uncertainty arises in the zero time of the modulation for very short distances. Variation of the zero time shifts the maximum of the distance distribution slightly (see Figure S19). This uncertainty of the mean distance, however, does not affect the conclusion of this work.

Table S1: Overview about experimental parameters used for NMR spectra

Experiment	**DARR *Hp*DnaB:AMP-PNP:Mg^{2+}**	**DARR *Hp*DnaB: AMP-PNP:Mn^{2+}**	**DARR BmrA: ADP:Mg^{2+}:VO_4^{3-}**	**DARR BmrA:ADP: Mn^{2+}:VO_4^{3-}**
MAS frequency/ kHz	17.0	17.0	17.5	17.5
Field/ T	20.0	20.0	18.8	18.8
Transfer I	HC-CP	HC-CP	HC-CP	HC-CP
^{1}H field/ kHz	60	60	70	70
X field/ kHz	42	42	53	53
Shape	Tangent ^{1}H	Tangent ^{1}H	Tangent ^{1}H	Tangent ^{1}H
^{13}C carrier/ ppm	103	103	100	100
Time/ ms	0.5	0.5		
Transfer II	DARR	DARR	DARR	DARR
^{1}H field/ kHz	17.0	17.0	17.5	17.5
^{13}C field/ kHz	-	-	-	-
^{15}N field/ kHz	-	-	-	-
Shape	-	-	-	-
Carrier/ ppm	103	103	100	100
Time/ ms	20	20	20	20
t1 increments	2560	2560	1875	1875
Sweep width (t1)/ kHz	100	100	93.75	93.75
Acquisition time (t1)/ ms	12.8	12.8	10	10
t2 increments	3072	3072	2802	2802
Sweep width (t2)/ kHz	100	100	93.75	93.75
Acquisition time (t2)/ ms	15.4	15.4	14.94	14.94
^{1}H Spinal64 decoupling power/ kHz	90	90	90	90
Interscan delay/ s	2.7	2.7	2.1	2.1
Number of scans	16	16	32	32
Measurement time/ h	32	32	36	36

Table S1 continued

Experiment	NCACB *Hp*DnaB:AMP-PNP:Mg^{2+}	NCACB *Hp*DnaB:AMP-PNP:Mn^{2+}
MAS frequency/ kHz	17.0	17.0
Field/ T	20.0	20.0
Transfer I	HN-CP	HN-CP
^{1}H field/ kHz	60	60
X field/ kHz	44	44
Shape	Tangent ^{1}H	Tangent ^{1}H
^{13}C carrier/ ppm	-	-
Time/ ms	0.7	0.7
Transfer II	NC-CP	NC-CP
^{1}H field/ kHz	-	-
^{13}C field/ kHz	6.0	6.0
^{15}N field/ kHz	10.6	10.6
Shape	Tangent ^{13}C	Tangent ^{13}C
Carrier/ ppm	58.3	58.3
Time/ ms	5.5	5.5
Transfer 3	DREAM	DREAM
^{1}H field/ kHz	-	-
^{13}C field/ kHz	7.3	7.3
^{15}N field/ kHz	-	-
Shape	Tangent ^{13}C	Tangent ^{13}C
Carrier/ ppm	55.9	55.9
Time/ ms	2	2
t1 increments	78	78
Sweep width (t1)/ kHz	6.0	6.0
Acquisition time (t1)/ ms	6.5	6.5
t2 increments	128	128
Sweep width (t2)/ kHz	8.8	8.8
Acquisition time (t2)/ ms	7.5	7.5
t3 increments	2304	2304
Sweep width (t3)/ kHz	100	100
Acquisition time (t3)/ ms	11.5	11.5
^{1}H Spinal64 decoupling power/ kHz	90	90
Interscan delay/ s	2.7	2.7
Number of scans	16	16
Measurement time/ h	121	121

Supplementary Figures

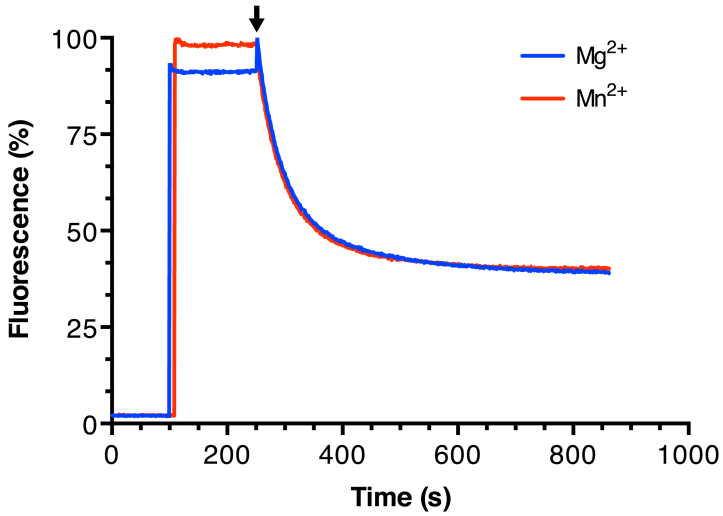

Figure S1: ATP-dependent transport of doxorubicin by inverted *E. coli* membrane vesicles. Addition of 10 µM doxorubicin with 100 µg of inverted membrane vesicles from *E. coli* C41(DE3) overexpressing BmrA incubated in presence of 2 mM ATP and ATP regeneration buffer (0-120 s). After addition of 10 µM doxorubicin (120 s), 2 mM of Mg^{2+} or Mn^{2+} was added, the addition of the metal ion is indicated by a black arrow. The transport activities of the ABC transporter show the same kinetic in presence of Mg^{2+} or Mn^{2+}.

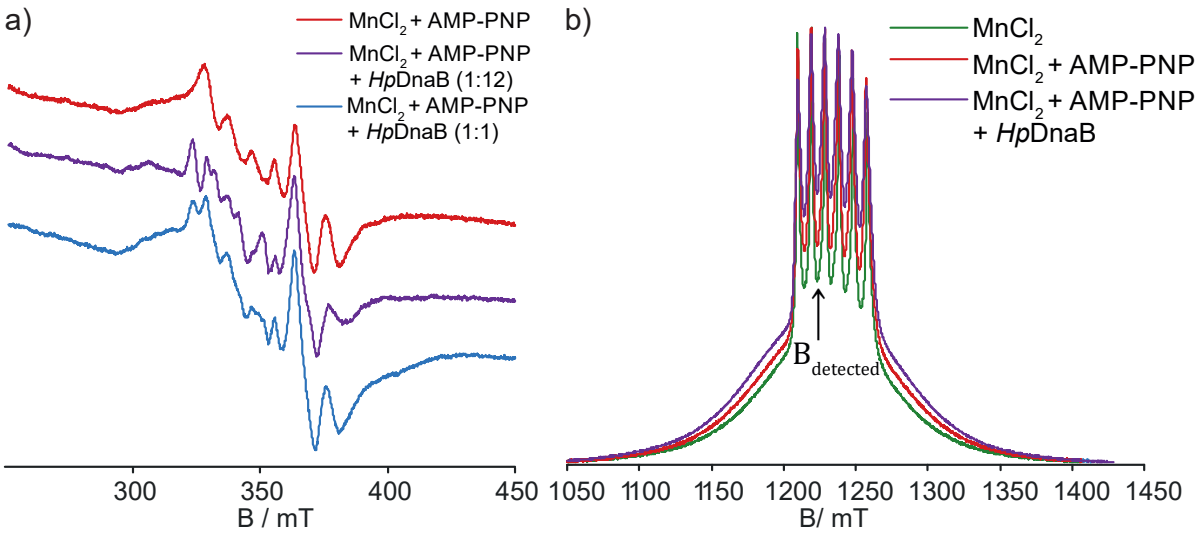

Figure S2: **(a)** Comparison of EPR CW line shapes for AMP-PNP:Mn^{2+} (red), 12:1 *Hp*DnaB:AMP-PNP:Mn^{2+} (purple) and 1:1 *Hp*DnaB:AMP-PNP:Mn^{2+} (blue) at r.t.. The spectrum of the sample with a 1:1 protein:Mn^{2+} ratio is a superposition of the spectrum of the AMP-PNP:Mn^{2+} sample and the sample with a 12:1 protein:Mn^{2+} ratio, thus indicating incomplete binding of Mn^{2+} to the NBDs in the case of a 1:1 protein:Mn^{2+} ratio. **(b)** Anisotropic broadening of EDEPR spectra at 20 K and 34.5 GHz indicating the binding of Mn^{2+} to *Hp*DnaB: EDEPR spectra of a 0.3 mM $MnCl_2$ solution in phosphate/D_2O/glycerol-d_8 buffer (green), a 0.3 mM $MnCl_2$, 5 mM AMP-PNP solution in phosphate/D_2O/glycerol-d_8 buffer (red) and a 0.3 mM $MnCl_2$, 5mM AMP-PNP, 0.3mM *Hp*DnaB phosphate/D_2O/glycerol-d_8 buffer (purple). In contrast to the room-temperature cw-EPR spectra in Figure 1, EDEPR experiments are performed in a frozen glassy matrix at 20 K and thus the spectral differences are dominated by changes in the zero-field splitting parameters, since molecular tumbling processes are frozen at these conditions. The observer field B_{detect} for relaxation and distance measurements is marked by an arrow.

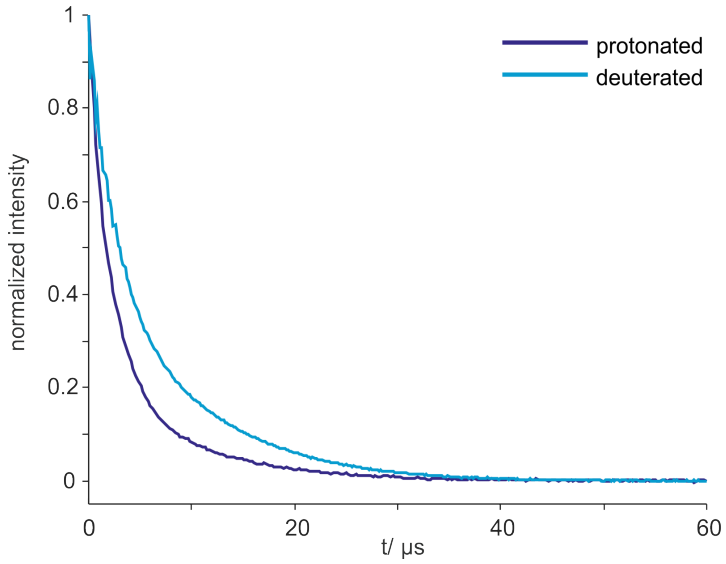

Figure S3: Hahn-echo decay of phase memory at a temperature of 20 K. Comparison of 0.3 mM *Hp*DnaB phosphate/D_2O/glycerol-d_8 buffer expressed in protonated (purple) or deuterated (cyan) media. Expression in deuterated media allows for longer DEER time traces, and, accordingly, to longer detectable Mn^{2+}-Mn^{2+}distances.

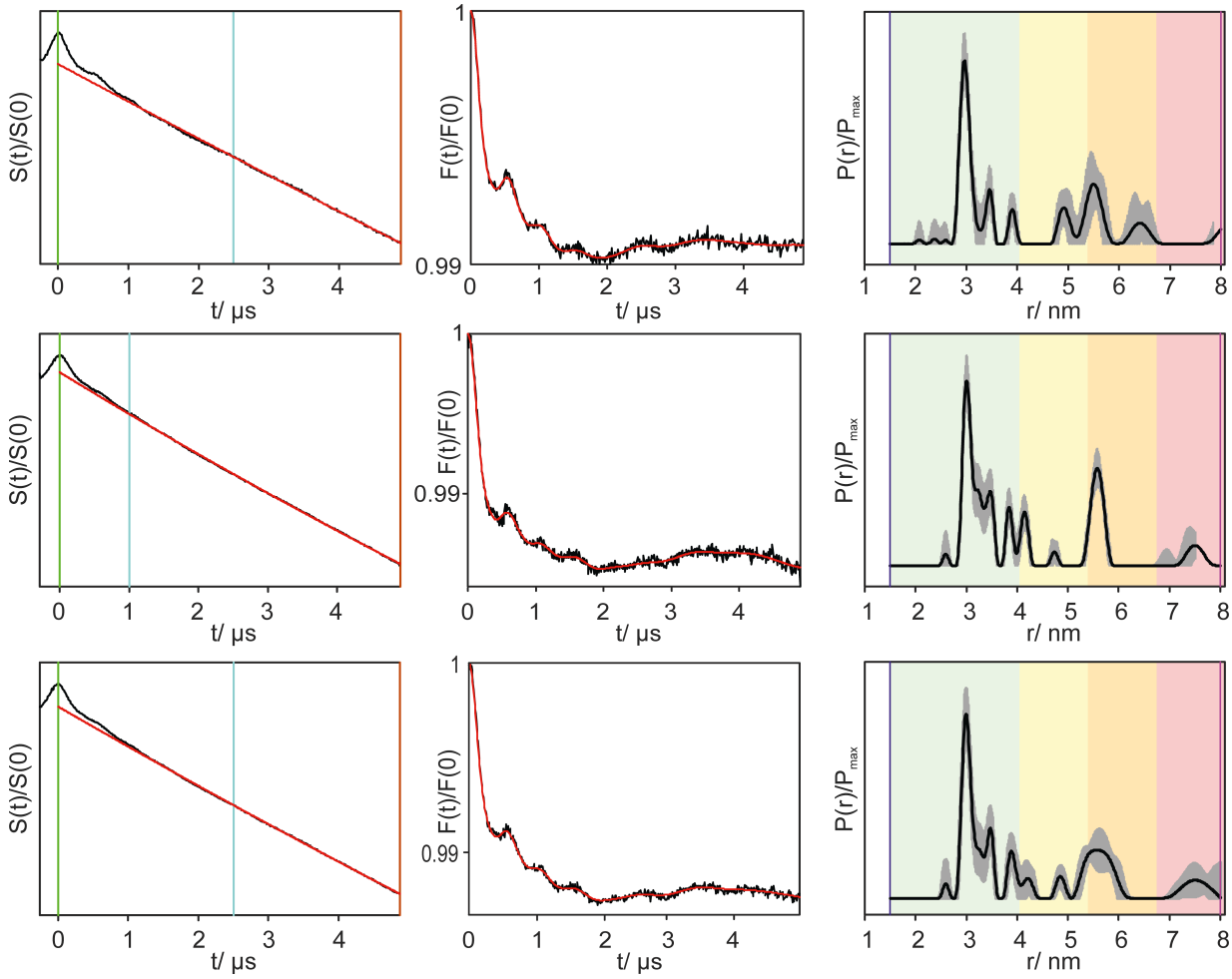

Figure S4: Overview of the Mn^{2+}-Mn^{2+} DEER data of *Hp*DnaB:AMP-PNP:Mn^{2+} expressed in deuterated media. Data sets from top to bottom: 800 MHz chirp pump pulse, 1200 MHz chirp pump pulse, average of both primary data sets. Left three panels: Normalized primary DEER data (black line) and background fit (red line). The zero time is marked by the green vertical line, the cyan line marks the beginning of the background range fit, and the orange line labels the cut-off position. Middle three panels: Background-corrected form factor in the time domain (black line) and corresponding fit (red line). Right three panels: distance distribution. The shaded areas give an error estimate if the start of the background fit range is varied from 1000 to 2500 ns and different artificial noise traces are added. The color-coding indicates reliability ranges resulting from the limited length of the dipolar evolution trace. Pale green: Shape of distance distribution is reliable. Pale yellow: Mean distance and width are reliable. Pale orange: Mean distance is reliable. Pale red: Long-range distance contributions may be detectable, but cannot be quantified (see DeerAnalysis manual).

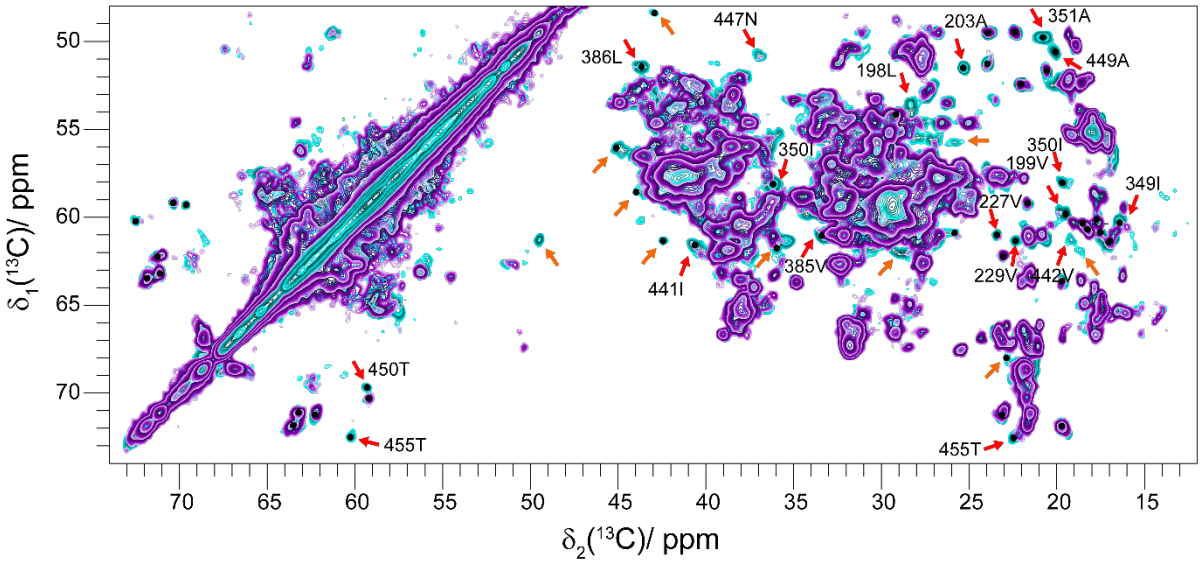

Figure S5: Most peaks experiencing chemical shift perturbations (CSPs) upon AMP-PNP:Mg^{2+} binding[10] are strongly attenuated or even disappearing in the *Hp*DnaB:AMP-PNP:Mn^{2+}-complex: Aliphatic region of ^{13}C-^{13}C 20 ms DARR spectra of the *Hp*DnaB:AMP-PNP:Mg^{2+} (18-fold excess Mg^{2+}, shown in cyan contours) and of the *Hp*DnaB:AMP-PNP:Mn^{2+} (5-fold excess Mn^{2+}, shown in purple contours) complexes. Strongly attenuated or even disappearing peaks are marked by red and orange arrows for assigned and unassigned peaks, respectively. Black circles indicate peaks experiencing CSPs > 0.15 ppm upon nucleotide binding compared to the isolated protein.

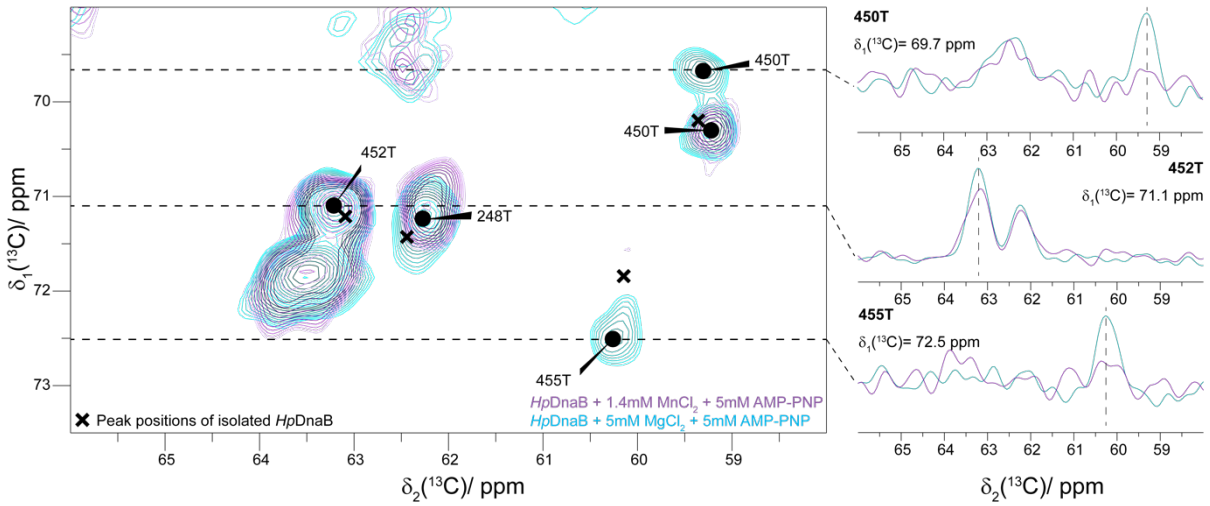

Figure S6: PRE effects influence 2D ^{13}C-^{13}C DARR spectra: Extract of threonine region from 2D ^{13}C-^{13}C DARR spectra of the *Hp*DnaB:AMP-PNP:Mg^{2+} (shown in cyan contours) and of the *Hp*DnaB:AMP-PNP:Mn^{2+} (shown in purple contours) complexes. Some representative 1D traces along F2 are shown as insets. Interestingly, from each of the doubled resonances for residues 449A[10] (see Figure 2 in the main text) and 450T only one signal (the one with large CSP) shows significant PRE, supporting the presence of two structurally slightly different NBDs, as also observed in the *Aa*DnaB:ADP:Mg^{2+} complex.

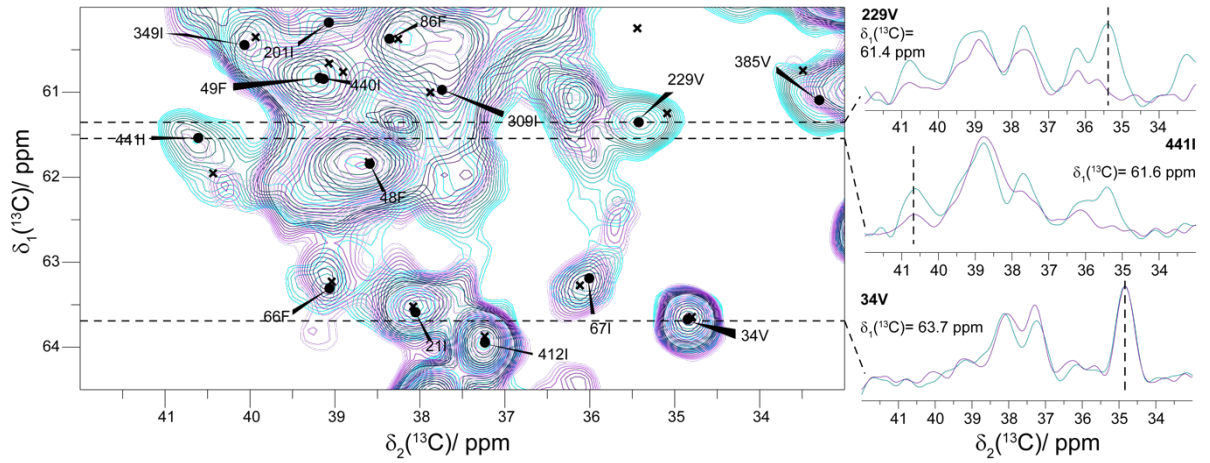

Figure S7: PRE effects influence 2D ^{13}C-^{13}C DARR spectra: Extract of isoleucine/valine region from 2D ^{13}C-^{13}C DARR spectra of the *Hp*DnaB:AMP-PNP:Mg^{2+} (shown in cyan contours) and of the *Hp*DnaB:AMP-PNP:Mn^{2+} (shown in purple contours) complexes. Some representative 1D traces along F2 are shown as insets.

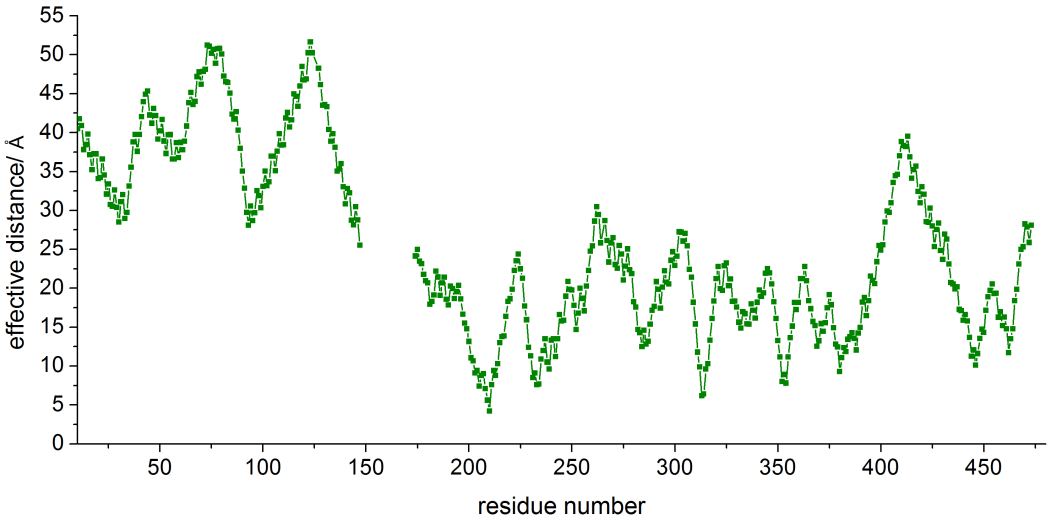

Figure S8: Effective distances between the protein and the metal center identify residues close to the NBD: Effective distances determined for *Hp*DnaB (calculated according to $\left(\sqrt[6]{\left(\frac{1}{d1}\right)^6+\left(\frac{1}{d2}\right)^6}\right)^{-1}$ with d_1 and d_2 representing the distance R between the metal ion and the Cα of the protein residue determined from the homology model). The measurements were performed on a homology model of *Hp*DnaB built from *Aa*DnaB:ADP:Mg^{2+}.[22] The residue numbers located at a difference smaller than 15 Å translate into the light red bars in Figure 2b in the main text.

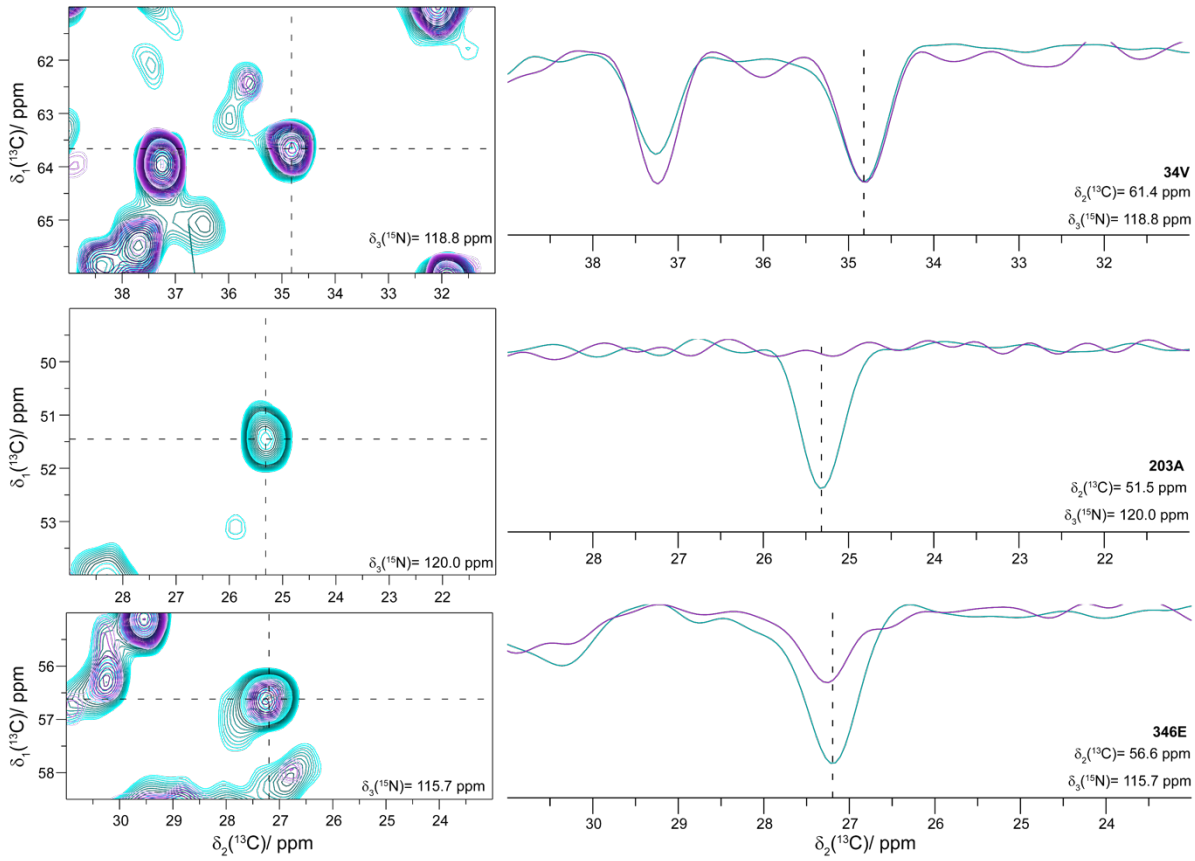

Figure S9: Site-specific determination of PRE effects from 3D spectra: Examples of 2D planes from 3D NCACB spectra of the *Hp*DnaB:AMP-PNP:Mg^{2+} (18-fold excess Mg^{2+}, shown in cyan contours) and of the *Hp*DnaB:AMP-PNP:Mn^{2+} (5-fold excess Mn^{2+}, shown in purple contours) complexes. Representative 1D traces along F2 are shown on the right.

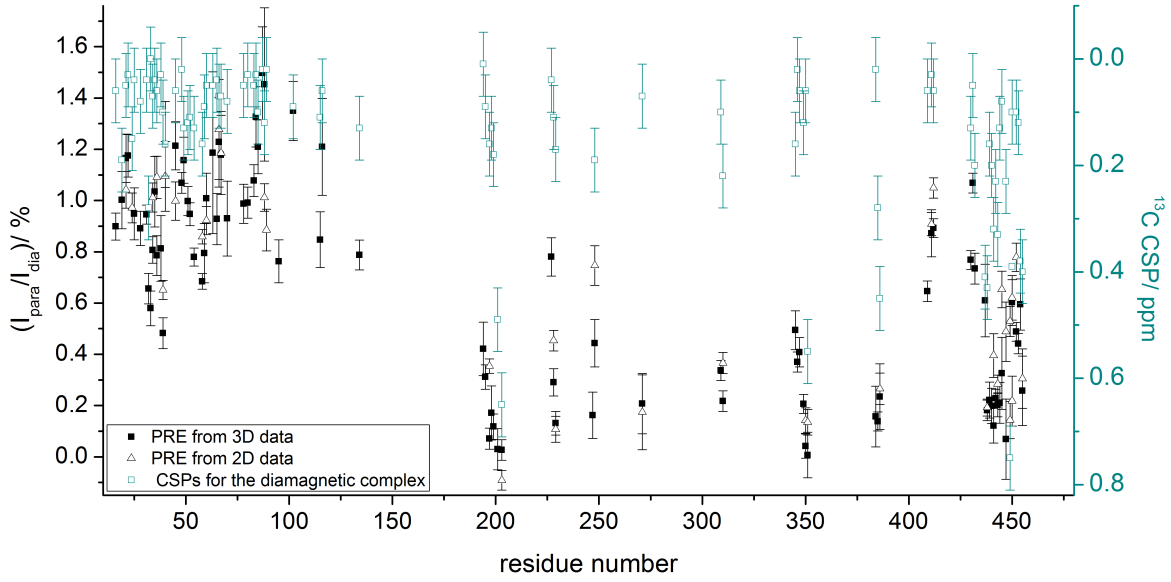

Figure S10: CSPs correlate with PRE effects: PRE effects (determined from 2D and 3D spectra shown as black squares and black triangles, respectively) are compared with ^{13}C CSPs for the diamagnetic *Hp*DnaB:AMP-PNP:Mg^{2+} complex (as reported in reference[10]). The comparison allows the following conclusions: (i) Residues showing detectable CSPs show also sizeable PRE effects and (ii) PRE effects serve as direct probes for helicase-nucleotide interactions, whereas ^{13}C CSPs rely on adaptions in the backbone geometry.

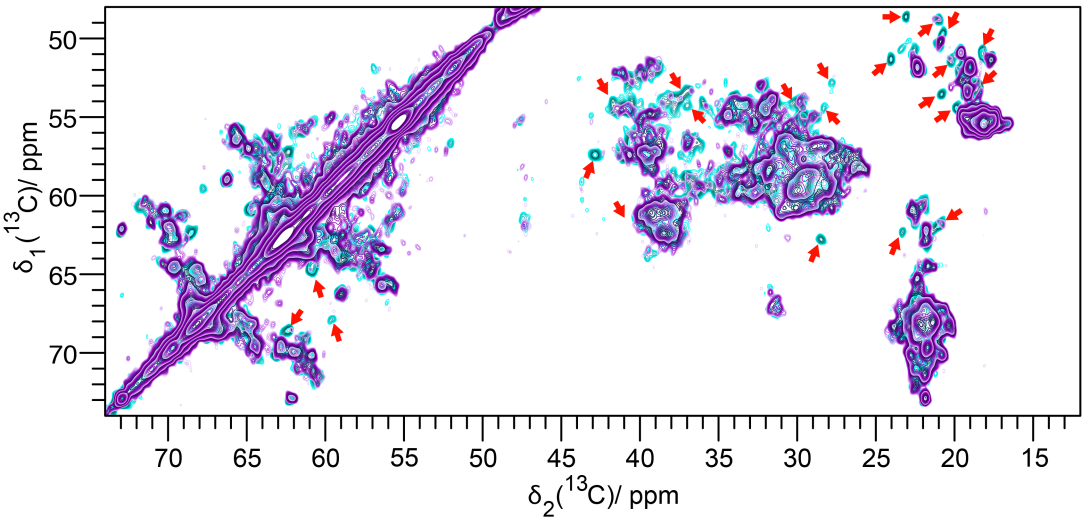

Figure S11: Aliphatic region from 2D ^{13}C-^{13}C DARR spectra of the reverse labeled ^{12}C-^{14}N-[LVIKHP]-^{13}C-^{15}N sample of BmrA:ADP:Mg^{2+}:VO_4^{3-} (shown in cyan contours) and of the BmrA:ADP:Mn^{2+}:VO_4^{3-} (shown in magenta contours) complexes. Strongly attenuated or disappearing peaks are marked by red arrows.

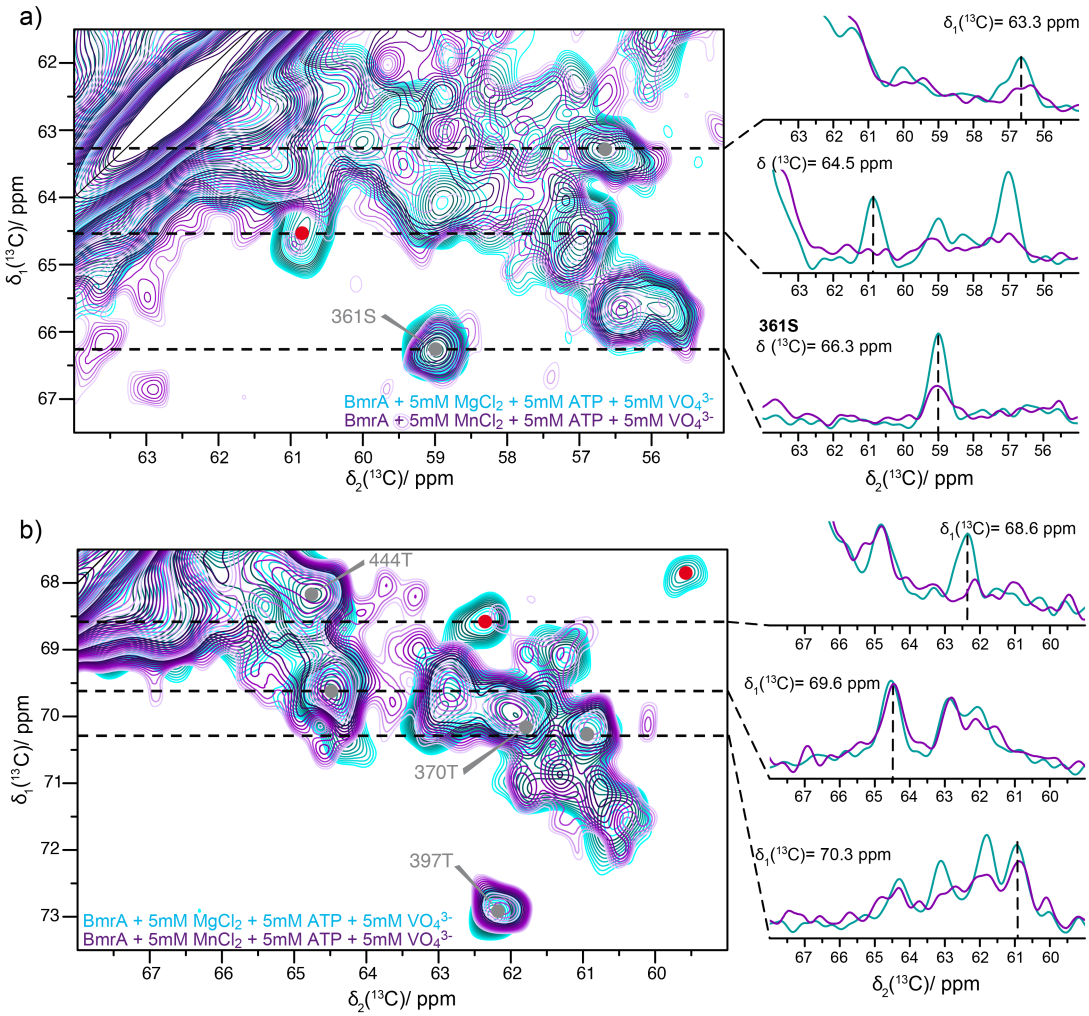

Figure S12: PRE effects influence 2D ^{13}C-^{13}C DARR spectra: Extract of threonine (**a**) and serine (**b**) region from 2D ^{13}C-^{13}C DARR spectra of the BmrA:ADP:Mg^{2+}:VO_4^{3-} (shown in cyan contours) and of the BmrA:ADP:Mn^{2+}:VO_4^{3-} (shown in magenta contours) complexes. Representative 1D traces along F2 are shown as insets for disappearing (black), and unaffected or attenuated resonances (grey).

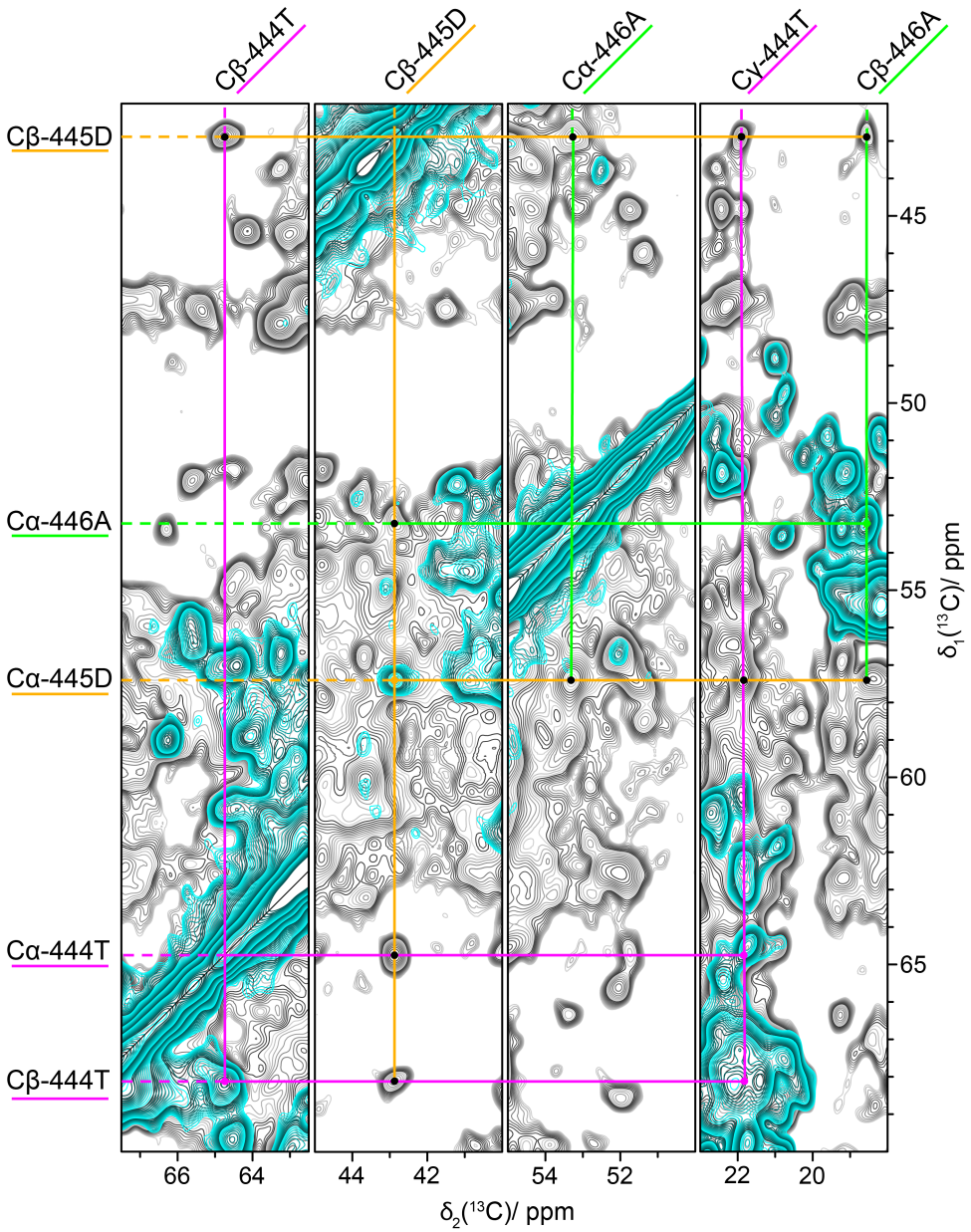

Figure S13: Example for amino acid assignments, showing residues 444T-445D-446A, using 2D ^{13}C-^{13}C DARRs recorded with 20 ms (cyan) and a 200 ms DARR (grey) mixing time on reverse labelled ^{12}C-^{14}N-[LVIKHP]-^{13}C-^{15}N BmrA:ADP:Mg^{2+}:VO_4^{3-}. Assignments were possible for amino acids showing isolated signals, clear amino-acid type signature, and sparse amino-acid type pairs or triples, as for example the TDA triple present only once in the BmrA sequence.

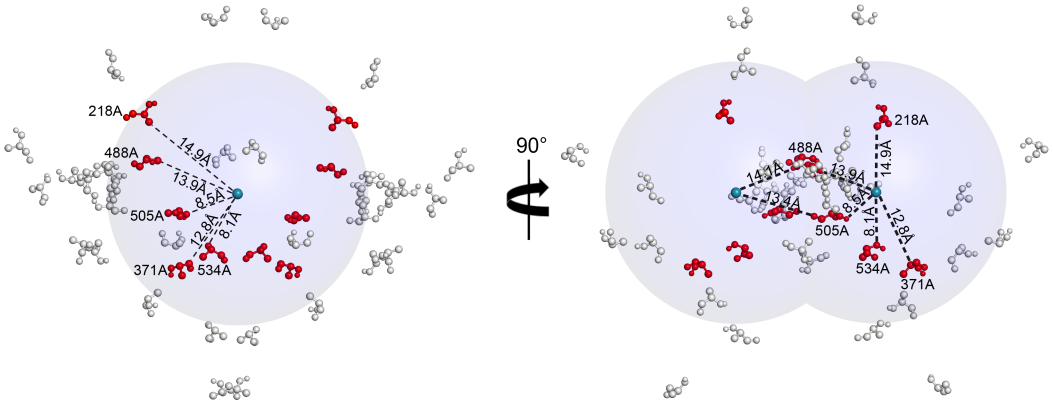

Figure S14: All alanine residues located in the nucleotide-binding domain of the BmrA model. The PREs effects from the two Mn^{2+} (highlighted in cyan) are shown by the spheres with a radius of 15 Å. The five alanine residues closer than 15 Å from the metal center are colored in red and their distances to the Mn^{2+} are indicated. The model used was obtained by homology from the ABC transporter SAV1866 x-ray structure (2HYD).[23]

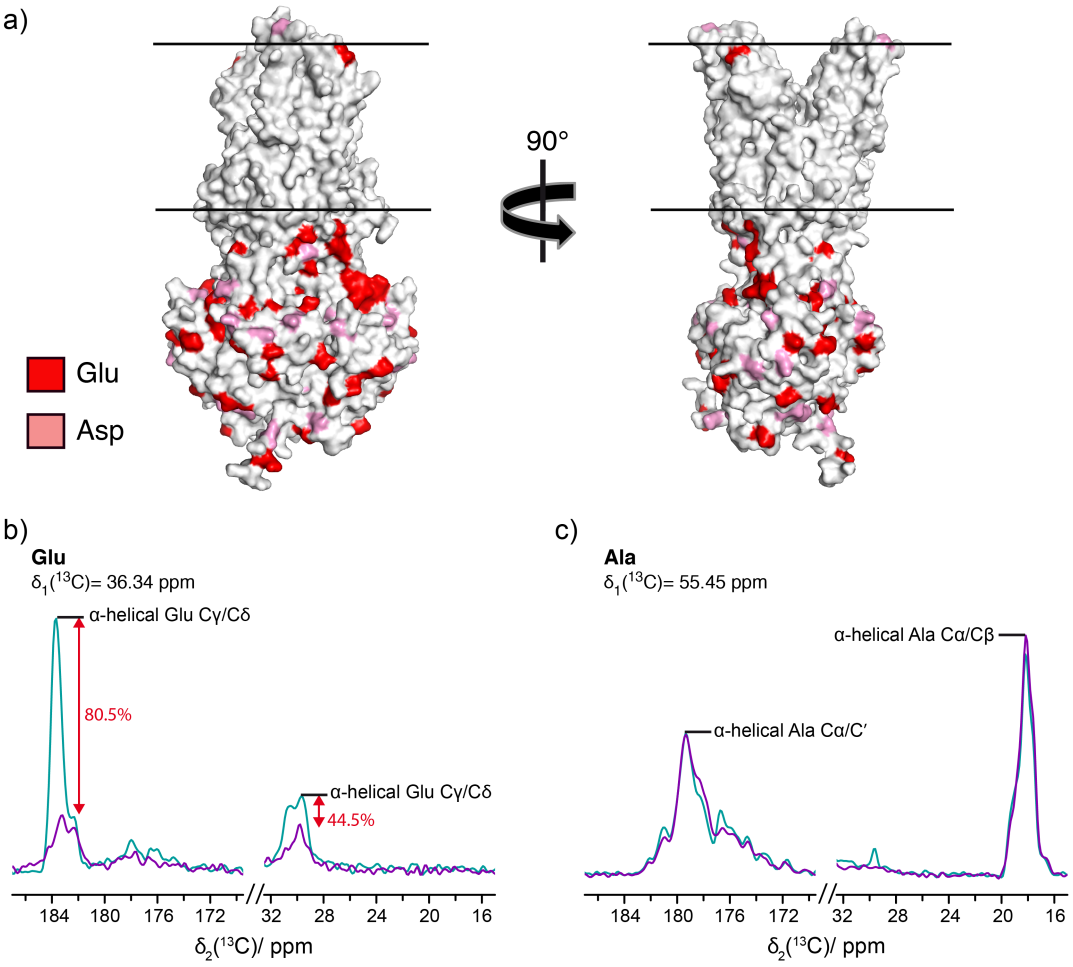

Figure S15: **a)** Glutamate and the aspartate residues are respectively plotted in red and pink on a homology model of BmrA (based on SAV1866 x-ray structure (2HYD)[23]), with the lipid bilayer represented by two solid black lines. **b)** and **c)** 1D traces of the glutamate (**b**) and alpha-helical alanine (**c**) residues of BmrA in presence of Mg^{2+} (cyan traces) and Mn^{2+} (magenta traces). The traces highlight the reduction of the signal from the glutamate residues induced by

the non-specific binding of the Mn^{2+} ions. In comparison, the 1D trace of the alpha-helical alanine residues, mainly protected by the lipid bilayer, are not affected.

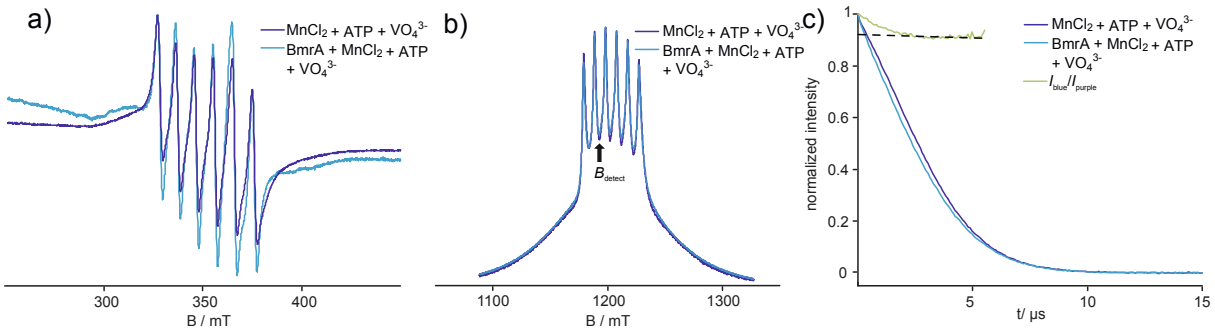

Figure S16: EPR data on BmrA and reference sample. **(a)** CW data for Mn^{2+} in the presence of ATP and VO_4^{3-} in BmrA buffer (magenta line) and the corresponding sample with BmrA added (cyan line) at r.t.. Note that the protein-containing sample was washed three times after incubation with Mn^{2+}, ATP and VO_4^{3-} (see Materials and Methods). The fraction of bound Mn^{2+} in BmrA is smaller compared to the Mn^{2+} in presence of AMP-PNP observed for the DnaB reference solution, and is spectroscopically closer to Mn^{2+} ions in buffer only (see Figure 1a in the main text). Nevertheless, upon addition of the protein a broader feature in the spectrum can be observed, indicating that a fraction of Mn^{2+} ions is bound. To test the stability of the formed complex, a single scan was detected before and after 1 hour of measurements. No significant spectral change was detected, indicating that the complex is stable for at least one hour. **(b)** EDEPR spectra detected at 10 K for Mn^{2+} ions in BmrA buffer with 50 % glycerol added (cyan line) for glass formation and the BmrA sample (magenta line) as described above. Only minor changes are observed in the protein sample, indicating that a large fraction of Mn^{2+} remained unbound. **(c)** Hahn echo decay at 10 K for the samples in b and their division trace (green line). The data show differential relaxation if the protein is present, and indicate that about 8 % of Mn^{2+} within the sample solution are bound.

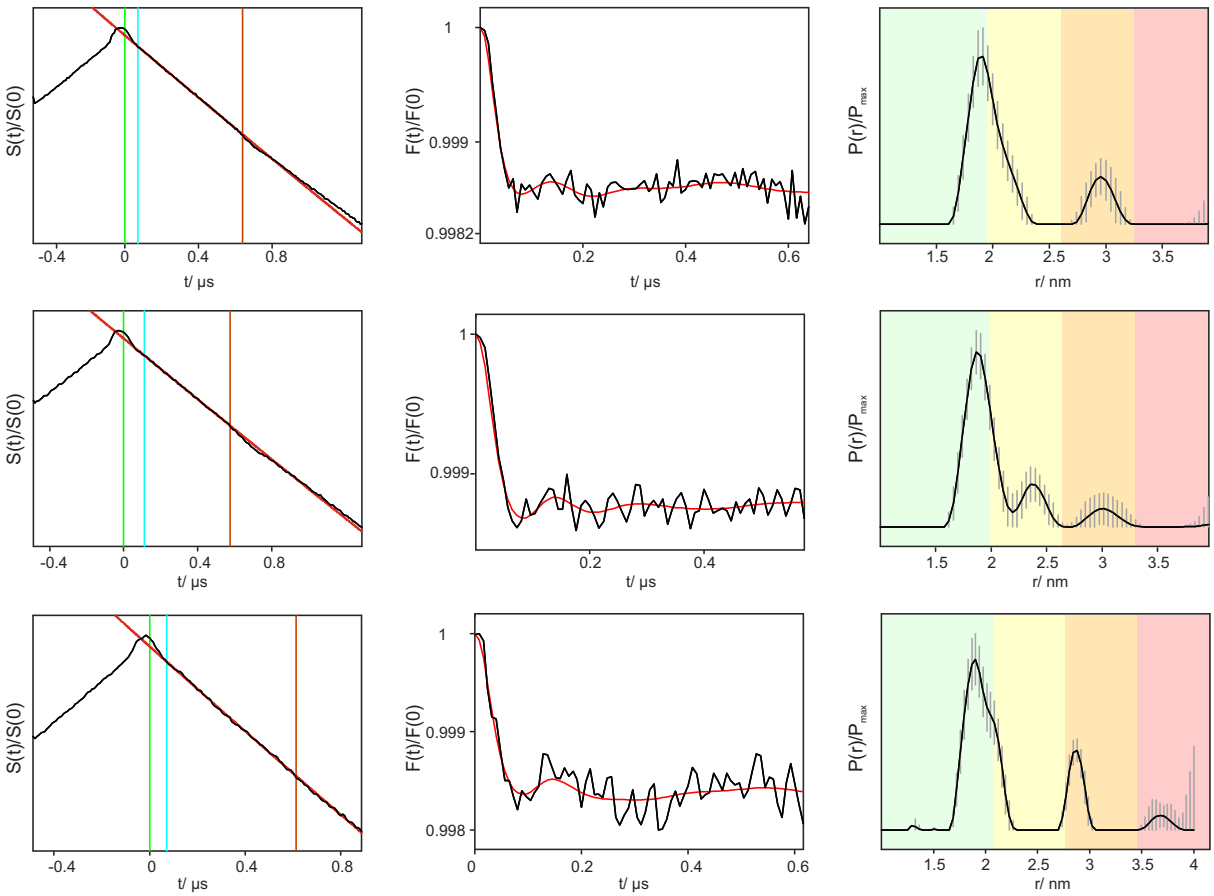

Figure S17: Overview of the Mn^{2+}-Mn^{2+} DEER data recorded on BmrA:ATP:Mn^{2+}:VO_4^{3-} at 10 K. Data sets from top to bottom: 1.2 GHz wide chirp pump pulse with 200 MHz offset between pump and observer frequency, 1.2 GHz wide chirp pump pulse with 300 MHz offset between pump and observer frequency and 0.8 GHz chirp pump pulse with 300 MHz offset between pump and observer frequency. Left three panels: Normalized primary DEER data (black line) and background fit (red line). The zero time is marked by the green vertical line, the cyan line marks the beginning of the background range fit, and the orange line labels the cut-off position. Middle three panels: Background-corrected form factor in the time domain (black line) and corresponding fit (red line). Right three panels: distance distribution. The shaded areas give an error estimate if the start of the background fit range is varied from 200 to 350 ns and different artificial noise traces are added. The color-coding indicates reliability ranges resulting from the limited length of the dipolar evolution trace. Pale green: Shape of distance distribution is reliable. Pale yellow: Mean distance and width are reliable. Pale orange: Mean distance is reliable. Pale red: Long-range distance contributions may be detectable, but cannot be quantified (see DeerAnalysis manual).

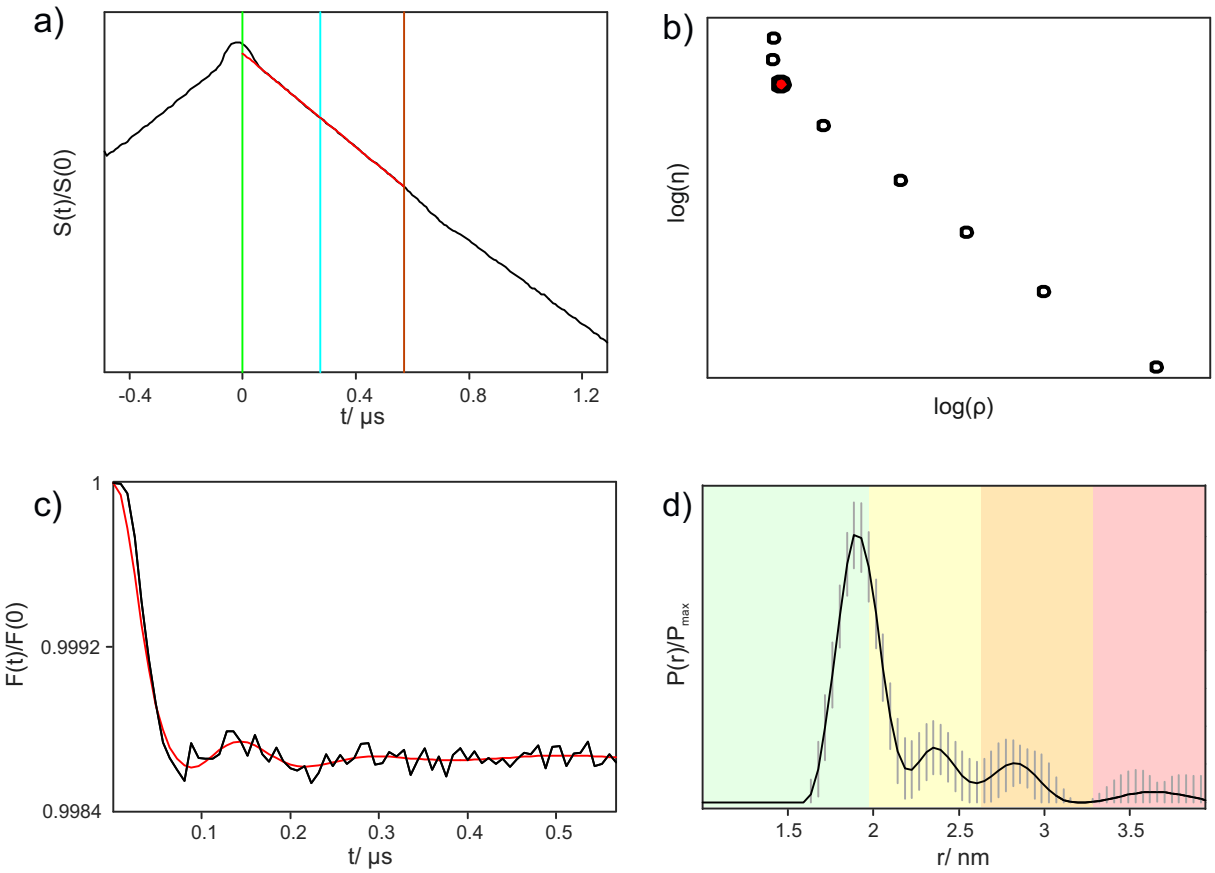

Figure S18: Overview of averaged Mn^{2+}-Mn^{2+} DEER data in BmrA:ATP:Mn^{2+}:VO_4^{3-} at 10 K. a) Primary data. The green vertical line marks the zero time, the cyan line the start of the background correction and the orange line the cut-off frequency, which is chosen based on artefacts occurring in the primary data (black line). The red line shows the background fit, b) L-curve resulting from Tikhonov regularization. The red dot marks the selected regularization parameter of 1, c) background corrected form factor (black line) and corresponding fit (red line), d) resulting distance distribution. The grey bands give an error estimate if the start of the background fit range is varied from 200 to 350 ns and different artificial noise traces are added. The color-coding indicates reliability ranges resulting from the limited length of the dipolar evolution trace. Pale green: Shape of distance distribution is reliable. Pale yellow: Mean distance and width are reliable. Pale orange: Mean distance is reliable. Pale red: Long-range distance contributions may be detectable, but cannot be quantified (see DeerAnalysis manual).

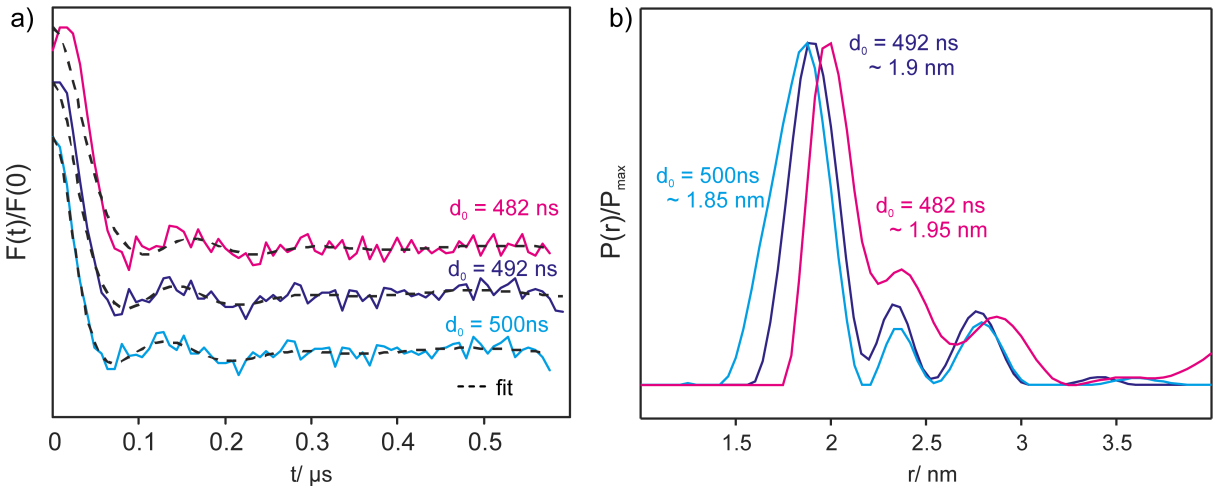

Figure S19: Variation of form factor **(a)** and distance distribution **(b)** upon change in zero time for the averaged data set shown in in Figure S18. The broader shape of the maximum in the primary data (see Figure S18) induces an uncertainty in the zero time. For very short distances this shifts the maximum of the distance distribution slightly. Setting the zero time to the theoretical value of 500 ns ($\tau_1 - t_{init}$, light blue line) gives a mean distance of about 1.85 nm, while placing the zero time rather symmetric around the maximum (~482 ns, magenta line) gives a mean distance of about 1.95 nm. This choice leads to a significant deviation between the measured (solid lines) and simulated DEER (black dashed lines) form factor. Placing the zero time to the start of the decay (~492 ns, violet line) results in a mean distance of about 1.9 nm, which we consider as the best estimate.

References

[1] C. Gardiennet, A. K. Schütz, A. Hunkeler, B. Kunert, L. Terradot, A. Böckmann, B. H. Meier, *Angew. Chem. Int. Ed.* **2012**, *51*, 7855–7858.

[2] I. Bertini, C. Luchinat, G. Parigi, E. Ravera, B. Reif, P. Turano, *Proc. Natl. Acad. Sci. USA* **2011**, *108*, 10396–10399.

[3] C. Gardiennet, T. Wiegand, A. Bazin, R. Cadalbert, B. Kunert, D. Lacabanne, I. Gutsche, L. Terradot, B. H. Meier, A. Böckmann, *J. Biomol. NMR* **2016**, *64*, 189–195.

[4] T. Wiegand, C. Gardiennet, F. Ravotti, A. Bazin, B. Kunert, D. Lacabanne, R. Cadalbert, P. Güntert, L. Terradot, A. Böckmann, et al., *Biomol NMR Assign* **2015**, 1–11.

[5] A. Böckmann, C. Gardiennet, R. Verel, A. Hunkeler, A. Loquet, G. Pintacuda, L. Emsley, B. H. Meier, A. Lesage, *J. Biomol. NMR* **2009**, *45*, 319–327.

[6] B. Kunert, C. Gardiennet, D. Lacabanne, D. Calles-Garcia, P. Falson, J.-M. Jault, B. H. Meier, F. Penin, A. Böckmann, *Front. Mol. Biosci.* **2014**, *1*, 5.

[7] E. Steinfels, C. Orelle, O. Dalmas, F. Penin, B. Miroux, A. Di Pietro, J.-M. Jault, *Biochim. Biophys. Acta* **2002**, *1565*, 1–5.

[8] T. J. Stevens, R. H. Fogh, W. Boucher, V. A. Higman, F. Eisenmenger, B. Bardiaux, B.-J. Rossum, H. Oschkinat, E. D. Laue, *J. Biomol. NMR* **2011**, *51*, 437–447.

[9] T. Wiegand, C. Gardiennet, R. Cadalbert, D. Lacabanne, B. Kunert, L. Terradot, A. Böckmann, B. H. Meier, *J. Biomol. NMR* **2016**, *65*, 1–8.

[10] T. Wiegand, R. Cadalbert, C. Gardiennet, J. Timmins, L. Terradot, A. Böckmann, B. H. Meier, *Angew. Chem. Int. Ed.* **2016**, *55*, 14164-14168.

[11] Y. Polyhach, E. Bordignon, R. Tschaggelar, S. Gandra, A. Godt, G. Jeschke, *Phys. Chem. Chem. Phys.* **2012**, *14*, 10762–10773.

[12] A. Doll, M. Qi, S. Pribitzer, N. Wili, M. Yulikov, A. Godt, G. Jeschke, *Phys. Chem. Chem. Phys.* **2015**, *17*, 7334–7344.

[13] P. Lueders, S. Razzaghi, H. Jäger, R. Tschaggelar, M. A. Hemminga, M. Yulikov, G. Jeschke, *Mol. Phys.* **2013**, *111*, 2824–2833.

[14] S. Razzaghi, E. K. Brooks, E. Bordignon, W. L. Hubbell, M. Yulikov, G. Jeschke, *ChemBioChem* **2013**, *14*, 1883–1890.

[15] A. Doll, M. Qi, N. Wili, S. Pribitzer, A. Godt, G. Jeschke, *J. Magn. Reson.* **2015**, *259*, 153–162.

[16] G. Hagelueken, W. J. Ingledew, H. Huang, B. Petrovic-Stojanovska, C. Whitfield, H. ElMkami, O. Schiemann, J. H. Naismith, *Angew. Chem. Int. Ed.* **2009**, *48*, 2904–2906.

[17] B. E. Bode, D. Margraf, J. Plackmeyer, G. Dürner, T. F. Prisner, O. Schiemann, *J. Am. Chem. Soc.* **2007**, *129*, 6736–6745.

[18] D. Banerjee, H. Yagi, T. Huber, G. Otting, D. Goldfarb, *J. Phys. Chem. Lett.* **2012**, *3*, 157–160.

[19] H. Y. Vincent Ching, P. Demay-Drouhard, H. C. Bertrand, C. Policar, L. C. Tabares, S. Un, *Phys. Chem. Chem. Phys.* **2015**, *17*, 23368–23377.

[20] S. Valera, K. Ackermann, C. Pliotas, H. Huang, J. H. Naismith, B. E. Bode, *Chem. Eur. J.* **2016**, *22*, 4700–4703.

[21] G. Jeschke, V. Chechik, P. Ionita, A. Godt, H. Zimmermann, J. Banham, C. R. Timmel, D. Hilger, H. Jung, *Appl. Magn. Reson.* **2006**, *30*, 473–498.

[22] M. S. Strycharska, E. Arias-Palomo, A. Y. Lyubimov, J. P. Erzberger, V. L. O'Shea, C. J. Bustamante, J. M. Berger, *Mol. Cell* **2013**, *52*, 844–854.
[23] R. J. P. Dawson, K. P. Locher, *Nature* **2006**, *443*, 180–185.